ВЫБРОС КОРОНАЛЬНОЙ МАССЫ И МЕЖПЛАНЕТНЫЕ МАГНИТНЫЕ ОБЛАКА
CORONAL MASS EJECTIONS AND INTERPLANETARY MAGNETIC CLOUDS

H. K. Biernat [1,2] , C. Möstl[1], M. Leitner[3], U. Taubenschuss[4], N. V. Erkaev[5], C. J. Farrugia[6]

[1] Space Research Institute, Austrian Academy of Sciences, Graz A-8042, Austria,
helfried.biernat@oeaw.ac.at

[2] Institute of Physics, University of Graz, A-8010, Austria

[3] Institute for Astro- and Particle Physics, University of Innsbruck, A-6020, Austria

[4] Department of Physics and Astronomy, University of Iowa, USA

[5] Institute of Computational Modelling, Russian Academy of Sciences, 660036 Krasnoyarsk-36, Russia

[6] Space Science Center and Dept. of Physics, University of New Hampshire, Durham, NH 03834, USA

Coronal mass ejections, the hurricanes of space, are massive expulsions of plasma and magnetic fields from the outer solar atmosphere into the interplanetary medium. Much effort in theoretical modeling and data interpretation is devoted to the understanding of their origin on the Sun, their interplanetary propagation, and their properties when they arrive at Earth as magnetic clouds.

In this report, we review on some recent developments in these areas of solar-terrestrial relations.

Introduction. Coronal mass ejections (CMEs) from the Sun, and their subsequent counterparts, interplanetary coronal mass ejections (ICMEs), observed in situ by spacecraft in the solar wind, are one of the most spectacular manifestations of solar activity. Magnetic clouds (MCs) (Burlaga et al. 1981) are those ICMEs which satisfy the definition of a higher than average magnetic field strength, a smoothly rotating magnetic field vector and low proton temperature. They are thought to form enormous loops, extending from the Sun into interplanetary space.

In this paper a review is given on various aspects of recent research on CMEs and magnetic clouds at the Space Research Institute in Graz, Austria in collaboration with Russian and US institutions. Basically, magnetic clouds are largescale (0.2 AU radial size near Earth) and expanding magnetic flux ropes detected in situ in the solar wind at all heliospheric distances. Three papers are discussed to show details on their observed evolution, numerical modeling of the interaction of the cloud with the ambient medium, and imaging observations by the new NASA STEREO mission covering the complete distance from the Sun to 1 AU.

In Leitner et al. (2007), 130 magnetic clouds (observed by the spacecraft Voyager, Pioneer, Helios, Wind and others) were modeled using a classic force-free modeling approach. From this, general laws on the MC expansion are derived. Numerical modeling by Taubenschuss et al. (2010) shows how reconnection between the outer MC magnetic fields with the solar wind influences the propagation of the MC. Finally, in Möstl et al. (2009), a case study is reported on the observations and modeling of a CME that has been tracked from the Sun to 1 AU using unique white light images of the solar wind from the new NASA STEREO mission.

For forecasting the geo-effectiveness of CMEs, i.e. their ability to drive geomagnetic storms, these results are essential, because MCs are known to be the strongest storm drivers. The reason is that their smoothly varying internal magnetic fields are able to produce strong and long lasting $-B_z$ (in the GSM coordinate system) intervals impinging the magnetopause. Research in this area is at a stage where observations, modeling and numerical simulation efforts are combined and compared to make the most progress.

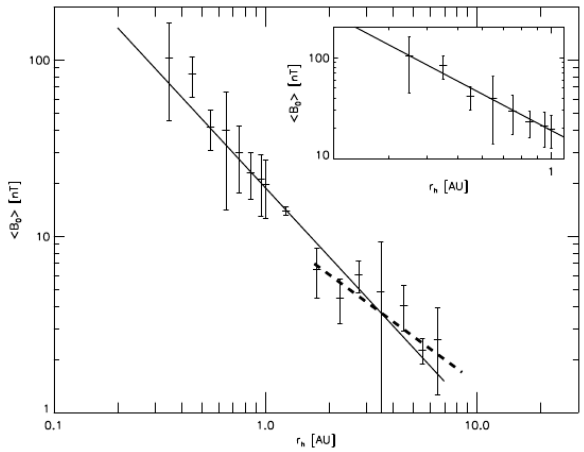

Fig. 1 - Double logarithmic plot of the fitted magnetic field strength inside magnetic clouds, averaged in each radial bin, versus heliospheric distance (Mean values with standard deviation for each r_h-bin). The solid line in the big panel gives a weighted curve fit ($w = 1/\sigma^2$) through all values, and the shorter dashed line is a fit for $r_h > 2$ AU. The inset shows a fit using values in $r_h \leq 1$ AU.

Force-free modeling and the evolution of magnetic clouds. Leitner et al. (2007) examined the implications of the widely used, force-free, constant-α flux rope model of interplanetary magnetic clouds to show the evolution of these transients.

Magnetic clouds are supposed to have a huge flux rope like geometry, which is expanding along its propagation through the interplanetary media. When sweeping over a spacecraft, a first approximation for modeling is to regard them as straight cylindrical objects, with a circular cross section. For such tubes there exists a solution for the shape of the magnetic field lines (Lundquist 1950), and such solutions can be fitted to the observations (Lepping et al. 1990). The Lundquist solution is given by terms of Bessel functions of zeroth and first order (J_0, J_1) and is a two component field in cylindrical coordinates (radial component vanishes) and given as

$$B_\alpha = B_0 J_0(\alpha R), \tag{1}$$

$$B_\Phi = H B_0 J_1(\alpha R) \tag{2}$$

with B_α the component along the axis of the cylinder (axial component), B_Φ the azimuthal component (tangential component), B_0 magnetic field strength in the center, H the helicity (±1, equal to right or left handed), α a constant given by $\alpha = 2.4/R_0$, with R_0 the radius of the cylinder, and R the radial distance from the axis of the cylinder $0 \le R \le R_0$.

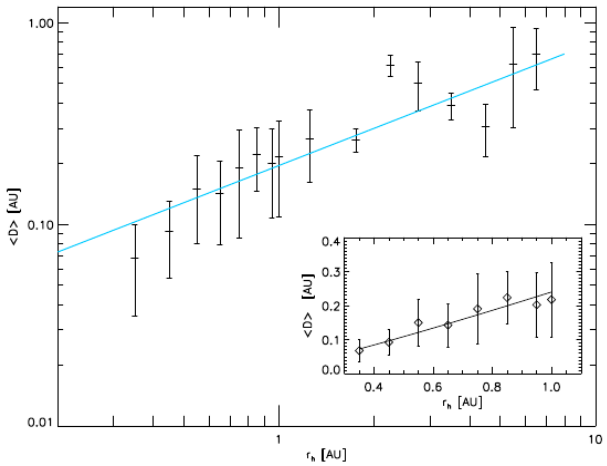

Fig. 2. - Average diameter of the magnetic cloud flux ropes versus heliospheric distance. Results in the inner heliosphere are shown on the inset (note the linear axes here). To obtain $\langle D \rangle$ the result from the least-squares fit is taken into account and is used to correct the simple $v \cdot t$ relation, which gives the apparent diameter.

A least squares fit is executed to obtain the magnetic field strength B_0, the orientation of the cylinder axis, an impact parameter p which gives the closest approach to the center and the sign of the helicity. A set of 130 magnetic clouds, mainly from Wind and Helios observations, were then studied and discussed based on the given model. Thus, the evolution of MCs as a function of heliospheric distance was given for the orientation of the axis, B_0, the tube size D, the density, the temperature, the plasma β and solar wind quasiinvariant.

Figure 1 gives the behavior of B_0 as a function of heliospheric distance r_h. While the large plot gives the result for all examined MCs the inset shows the results just for the inner heliosphere. The solid lines are fits of the type $y = a \cdot r_h^b$, which are weighted by the inverse squared standard deviation w = $1/\sigma^2$. For all values, this yields (B_0 in nT and r_h in AU),

$$\langle B_0 \rangle = (18.8 \pm 1.4) \cdot r_h^{(-1.30 \pm 0.09)} \tag{3}$$

and for the inner heliosphere we have

$$\langle B_0 \rangle = (18.1 \pm 3.8) \cdot r_h^{(-1.64 \pm 0.40)} \tag{4}$$

The functional dependence $\langle D \rangle (r_h)$ is shown in Figure 2, and the inset (note the linear scales) shows again the results for the inner heliosphere. The fit through all averaged events is (D and r_h both in AU)

$$\langle D \rangle = (0.195 \pm 0.017) \cdot r_h^{(0.61 \pm 0.087)} \tag{5}$$

and the result for the inner heliosphere is

$$\langle D \rangle = (0.23 \pm 0.05) \cdot r_h^{(1.14 \pm 0.44)} \tag{6}$$

The radial behavior of B_0 and D show both a kink in the profiles which appear at about r_h = 2 AU, suggesting that for r_h > 2 AU, $\langle B_0 \rangle$ and $\langle D \rangle$ decrease less rapidly than in the inner heliosphere. This may be a spurious result due to poor statistics for high r_h. If so, this can be remedied by taking more events.

However, its cause may be more fundamental. In past work on a self-similarly expanding flux rope model (e.g. Farrugia et al. 1993), it was argued that the axial and azimuthal components of the flux rope field depend differently on r_h, the axial field B_α decreasing as $B_\alpha \propto 1/r_h^2$, and the azimuthal field as $B_\Phi \propto 1/r_h$. In this model, therefore, as time from ejection at the Sun (and r_h) increases, the decline in B_0 becomes increasingly determined by that of B_Φ, leading to a slower decrease at large r_h. This might be the cause of the kink.

Ideal MHD simulations and the role of magnetic handedness. During propagation, magnetic clouds interact with the structured ambient solar wind (e.g. the fast wind emanating from the polar coronal holes) leading to substantial distortion and deformation. Taubenschuss et al. (2010) have studied these effects in the frame of ideal magnetohydrodynamic (MHD) simulations. In ideal MHD, the solar wind plasma can be described by a set of eight nonlinear first-order partial differential equations (PDEs) of the hyperbolic type (Toro 1999; LeVeque 2002). This set comprises the conservation equations for mass density, momentum density, magnetic induction and energy density (Powell et al. 1999). For a numerical solution, the computational domain is divided into a 2-D spherical polar grid of cells ranging in radial direction from the outer regions of the solar corona at 0.05 AU up to a distance beyond Earth (1.75 AU). The second dimension either creates an equatorial or a meridional plane depending on the investigated scenario of MC propagation. So, actually the propagation of a 2-D cross section of the magnetic cloud through the inner heliosphere is the subject to MHD simulations. Each cell of the grid is interpreted as a "finite volume". Numerical fluxes between the cells are computed on the basis of solutions to a local Riemann problem (Godunov 1959). Furthermore, instead of solving the original nonlinear system of PDEs, a Roe-type approximate Riemann solver is applied to the linearized version of the system (Roe 1981; Brio & Wu 1988; Zachary & Colella 1992). Eigenvalues and eigenvectors for the linearized system have already been calculated by Powell (1994) in terms of the primitive variables, i.e. , mass density, bulk velocity, magnetic induction, and thermal pressure.

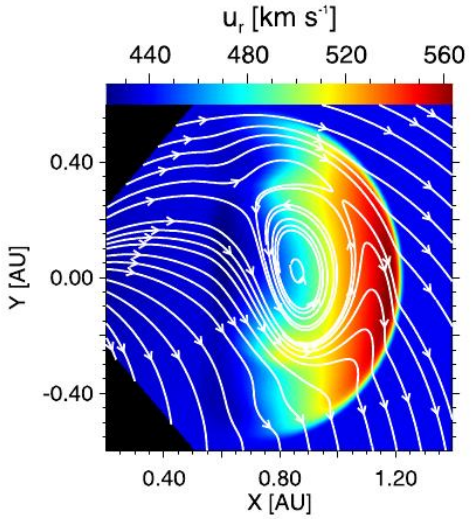

Fig. 3. - The simulated MC's cross section in the equatorial plane after several hours of propagation from the outer solar corona to a distance of 1 AU. Radial velocities are shown in rainbow colors. Projections of magnetic field lines into the equatorial plane are over-plotted in white. They reveal the MC's elliptical shape. The fast-mode shock ahead of the MC is evident according to the jump in solar wind speed. Magnetic reconnection between the MC and the IMF takes place in the front side sheath at positive y-coordinates.

Four different scenarios of initial MC configurations have been simulated with special emphasis placed on the role of the initial magnetic handedness or sign of the helicity (H = +1 or H = -1, see Equations (1) and (2)). The initial magnetic handedness strongly influences the efficiency of magnetic reconnection between the MC's magnetic field and the interplanetary magnetic field. All four propagation scenarios, i.e., the two equatorial and the two meridional ones, comprise the following common features: Strong expansion during propagation, low values for the plasma-β inside the MC, deceleration towards the speed of the ambient solar wind, a fast mode shock and a sheath ahead of the MC, and strong deformation of the initial circular cross section.

The propagation of an MC with its axis oriented perpendicular to the equatorial plane leads to a transformation from the initial circular shape into an elliptic one. Expansion turns out to be stronger into the direction perpendicular to the direction of propagation, i.e., into the azimuthal direction (see Fig. 3). Furthermore, MHD simulations reveal that the whole cross section is drifting along the azimuthal direction (~ 0.04 AU during a radial propagation range of 1 AU). The drift motion is caused by an acceleration of MC plasma in the azimuthal direction towards the reconnection site. Depending on the MC's handedness, magnetic reconnection between the MC and the Parker spiral IMF either occurs on the front side or on the backside. Fig. 3 presents the results obtained for a magnetic cloud near 1 AU. It is released with a circular cross section and a H = +1 near the Sun, but it gets transformed into an elliptic

shape while propagating outward. Magnetic reconnection occurs inside the sheath in front of the MC as can be seen according to the contours of projected magnetic field lines.

An orientation of the MC's axis parallel to the equatorial plane leads to a concave-outward shape for the meridional cross section. The bi-modal ambient solar wind is modeled to be typical for a solar activity minimum with higher wind speeds at higher heliographic latitudes (see Fig. 4). The initial magnetic handedness of the MC determines how the MC starts to interact with the interplanetary magnetic field. This is of vital importance especially at the front side shock and sheath because it determines the orientation of the sheath's magnetic field, and thus influences the MC's geoeffectiveness at Earth.

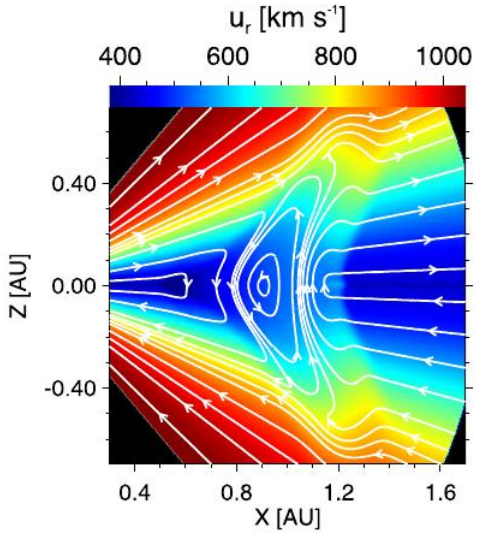

Fig. 4. - Speeds and magnetic field orientations for the meridional propagation scenario. The magnetic handedness (H = +1) of the cloud forces IMF field lines to be reconnected across the heliospheric current sheet in front of the MC and behind the MC. Furthermore, there is significant magnetic reconnection visible between the MC and the IMF along the rear flanks where magnetic field orientations are antiparallel. Note the concave-outward shape of the MC and the bimodal speed pattern for the solar wind as a function of latitude.

Depending on the handedness, IMF field lines are either turned around the MC body or they become reconnected across the heliospheric current sheet.

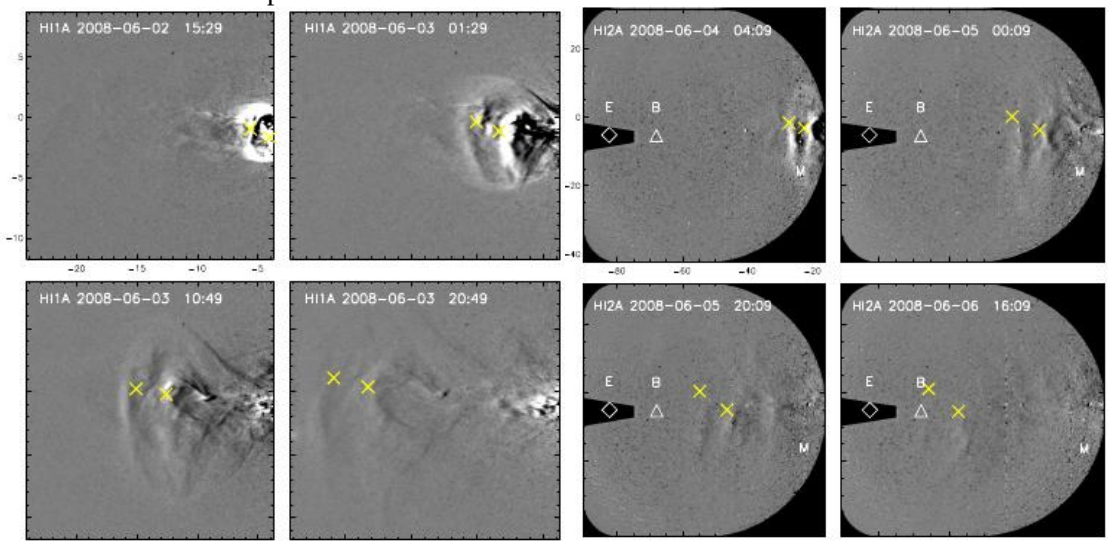

Fig. 5. - Evolution of the June 1-6 CME seen by STEREO-A (HI1, left 4 images and HI2, right 4 images). Earth (E), STEREO-B (B) are indicated as well as the elongation of Mercury (M). The CME leading edge and core for Fig. 6 are marked by yellow crosses.

The presence of an equatorward flow of plasma showing up in front of concave-outward shaped magnetic clouds could be confirmed (Manchester et al. 2005; Liu et al. 2008). MHD simulations reveal that equatorward flows develop independently of the magnetic handedness of the MC, and they seem to be a direct consequence of the shape of the cloud's shock front. The maximum amplitude derived for these flows is rather low (< 20 km s^{-1}), but would increase with increasing curvature for the MC and its front side shock.

Finally, the issue of force-free magnetic fields is also addressed by (Taubenschuss et al. 2010). The degree of force-freeness is parameterized, and its evolution is pursued during propagation of the MC

from the inner boundary up to the distance of Earth. Despite the strong deformation of the cross section, an initial force-free configuration for magnetic clouds seems to be conserved very well, at least in an average sense since we average over the whole cross-section.

Observations of a coronal mass ejection from the Sun to 1 AU. Möstl et al. (2009) presents for the first time the relationship between a CME observed from the Sun to 1 AU and the flux rope orientation derived from modeling the in situ magnetic field and plasma observations. The observations where done with both of the new NASA STEREO spacecraft (launched in October 2006) of a CME from 1-6 June 2008. The two observatories are orbiting the Sun close to 1 AU in the ecliptic plane. The orbits were chosen in such a way that one increasingly lags the Earth due to a slightly larger heliocentric distance (accordingly called STEREO-Behind) and the other one (STEROE-Ahead) is separating from Earth in the direction of Earth's orbit (Kaiser et al. 2008). Every year the two STEREO spacecraft separate by about 44 degrees in longitude. Besides other instruments, STEREO is equipped with two novel "Heliospheric imager" (HI) cameras on each spacecraft (Eyles et al. 2009). For the first time, it is possible to image the solar wind density for the complete Sun-Earth line. The physics behind this is continuous Thomson scattering of white light with free electrons in the hot and mostly ionized solar wind (Vourlidas & Howard 2006).

On June 1-6 2008, an intriguing coronal mass ejection, blown out along a helmet streamer, has been observed by STEREO-A. It did not have any accompanying signatures, like a flare, on the solar surface (Robbrecht et al. 2009). The CME was directed toward STEREO-B, separated to STEREO-A about 55 degrees in longitude. The CME direction was inferred by Möstl et al. (2009) using four different techniques. Figure 5 shows images from the STEREO-Ahead HI camera with the CME being observed as two bright fronts sweeping through the inner heliosphere - the earlier one (left X in Fig. 5) is called the CME's leading edge, and the second one the CME core.

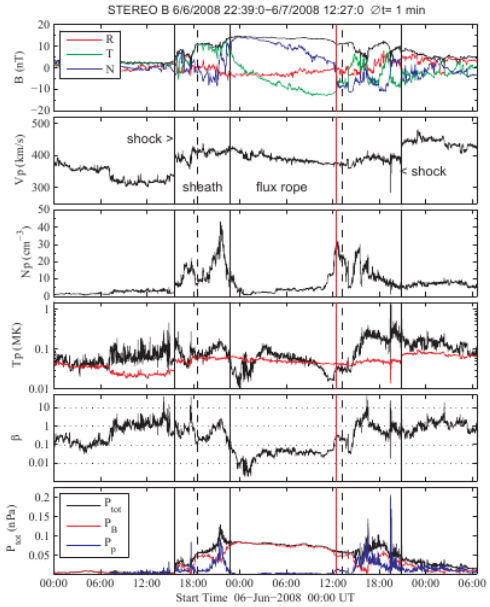

Fig. 6. - Magnetic field and plasma data (STEREO-B). Two outer solid lines indicate the forward and reverse shock. Dashed lines are the arrival time of the CME leading edge (left) and core (right). From top to bottom: magnetic field magnitude and magnetic field components in RTN coordinates, proton bulk velocity, proton number density, proton temperature (black) and expected temperature (red), proton beta and the total, magnetic and plasma pressure.

The position of the STEREO-B spacecraft is also indicated in the lower four images. It is seen in a straightforward way that the leading edge is at the same elongation angle as STEREO-B around 16:00 UT, June 6, 2008.

In Figure 6, a plot showing the in situ data observed directly in the solar wind with the STEREO-B instruments PLASTIC (proton bulk parameters; Galvin et al. 2008) and IMPACT (magnetic field components; Luhmann et al. 2008) is presented. Indeed, the first density wave in Figure 5 (equal to the CME leading edge) is associated with a strong rise in the solar wind proton density, from less than 5 protons/ccm to 20-40 protons/ccm. The transition is delineated in the front by a shock wave, accompanied by jumps in the magnetic field components, density, temperature and velocity. After the first density enhancement, signatures of a large-scale magnetic flux rope are observed, including a rotating magnetic field vector, but not a clearly lower proton temperature which precludes the flux rope from being a magnetic cloud. The magnetic field signature is consistent with an orientation of a cylindrical flux rope with its axis tilted roughly 45 degrees to the ecliptic (for details and modeling see Möstl et al. 2009). The

second density peak, i.e. the CME core, arrived only after the flux rope has ended and was accompanied by a more irregular magnetic field, but might include another, though much smaller flux rope.

Conclusions. Leitner et al. (2007) have modeled a large set of magnetic clouds to find general laws on their expansion, extending the famous study by Bothmer & Schwenn (1998). Taubenschuss et al. (2010) presented results gained from MHD simulations which turned out to reflect quite well the picture for magnetic clouds which has been derived from long-term in-situ observations.

One big disadvantage of in-situ observations is that they are performed just along a single path, and an additional model is always required to get a more global picture of physical relationships. The global solution obtained from MHD simulations enables a detailed parameterization of the evolution of important quantities in the whole computational domain. Thus, they serve as a basis under more general conditions in order to support the interpretation of in-situ observations. Particularly the effects of different magnetic handedness for magnetic clouds have been elaborated clearly here. The consequences of magnetic reconnection between the magnetic cloud and the interplanetary magnetic field became evident. Another way to directly see the evolution of CMEs and MCs is to use the new heliospheric imager instruments on the two NASA STEREO satellites (Möstl et al. 2009). This showed that it is indeed possible to image CMEs all the way from the Sun to the Earth owing to intelligent instrument design which makes use of the physics of Thomson scattering.

In conclusion, we see that combining different types of research, both data-driven and by using numerical simulations, is probably the best way to make progress in this area. The research presented here is aimed at enhancing our basic level of understanding, but will nevertheless help one day to enhance our ability to forecast disturbances of the Earth's magnetosphere, detrimental to some key parts of mankind's technology, for some days in advance.

Acknowledgements. We acknowledge the Austrian Science Fund (FWF) under Projects P20145-N16 and I193-N16. This work is supported by NASA grants NAS5-00132, NNG06GD41G and NNX08AD11G. We thank the STEREO/SECCHI and Wind SWE/MFI teams for their open data policy.

Bibliography

1. Bothmer, V., & Schwenn, R. 1998, Annales Geophysicae, 16, 1
2. Brio, M., & Wu, C. C. 1988, Journal of Computational Physics, 75, 400
3. Burlaga, L., Sittler, E., Mariani, F., & Schwenn, R. 1981, J. Geophys. Res., 86, 6673
4. Eyles, C. J., et al. 2009, Sol. Phys., 254, 387
5. Farrugia, C. J., Burlaga, L. F., Osherovich, V. A., Richardson, I. G., Freeman, M. P., Lepping, R. P., & Lazarus, A. J. 1993, J. Geophys. Res., 98,7621
6. Galvin, A. B., et al. 2008, Space Science Reviews, 136, 437
7. Godunov, S. K. 1959, Mat.Sb.
8. Kaiser, M. L., Kucera, T. A., Davila, J. M., St. Cyr, O. C., Guhathakurta, M., & Christian, E. 2008, Space Science Reviews, 136, 5
9. Leitner, M., Farrugia, C. J., Möstl, C., Ogilvie, K. W., Galvin, A. B., Schwenn, R., &Biernat, H. K. 2007, Journal of Geophysical Research (Space Physics), 112, 6113
10. Lepping, R. P., Burlaga, L. F., & Jones, J. A. 1990, J. Geophys. Res., 95, 11957
11. LeVeque, R. J. 2002, Finite volume methods for hyperbolic problems, (Cambridge University Press)
12. Liu, Y., Manchester, W. B., Richardson, J. D., Luhmann, J. G., Lin, R. P., & Bale, S. D. 2008, Journal of Geophysical Research (Space Physics), 113, 0
13. Luhmann, J. G., et al. 2008, Space Science Reviews, 136, 117
14. Lundquist, S. 1950, Ark. Fys.
15. Manchester, IV, W. B., et al. 2005, ApJ, 622, 1225
16. Möstl, C., Farrugia, C. J., Temmer, M., Miklenic, C., Veronig, A. M., Galvin, A. B., Leitner, M., & Biernat, H. K. 2009, ApJ, 705, L180
17. Powell, K. G. 1994, Approximate Riemann solver for magnetohydrodynamics (that works in more than one dimension), Tech. rep., NASA Langley Research center
18. Powell, K. G., Roe, P. L., Linde, T. J., Gombosi, T. I., & de Zeeuw, D. L. 1999, Journal of Computational Physics, 154, 284
19. Robbrecht, E., Patsourakos, S., & Vourlidas, A. 2009, ApJ, 701, 283
20. Roe, P. L. 1981, Journal of Computational Physics, 43, 357
21. Taubenschuss, U., Erkaev, N. V., Biernat, H. K., Farrugia, C. J., Möstl, C., & Amerstorfer, U. V. 2010, Annales Geophysicae, submitted
22. Toro, E. F. 1999, Riemann solvers and numerical methods for fluid dynamics (Springer - Berlin, Heidelberg)
23. Vourlidas, A., & Howard, R. A. 2006, ApJ, 642, 1216
24. Zachary, A. L., & Colella, P.1992, Journal of Computational Physics, 99, 341